Fast Centralized Model Predictive Control for Wave Energy Converter Arrays Based on Rollout

Zechuan Lin, Xuanrui Huang, Yifei Han, Xi Xiao, *Member, IEEE*, and John V. Ringwood, *Fellow, IEEE*

***Abstract*—Centralized control of wave energy converter (WEC) arrays for grid-scale generation can achieve higher energy production than decentralized (independent) control, due to its capability of fully exploiting mutual radiation effects. However, the state-of-the-art centralized model predictive control (CMPC) is significantly more computationally challenging than decentralized MPC (DMPC), since the number of control moves to be optimized grows in proportion to the number of WECs. In this paper, a fast CMPC controller is proposed, whose idea is to optimize only the first few control moves while rolling out future system trajectories using a fixed controller. A linear, two-degree-of-freedom (2-DoF) controller with a sea-state-dependent control coefficient tuning strategy is further proposed to serve as the rollout controller. It is shown that the proposed rollout-based CMPC (R-CMPC) can maintain almost the same energy production as conventional CMPC under a wide range of sea states, while significantly reducing the optimization dimension (in the studied case, by a factor of 6), enabling ultra-fast online computation (about 40 times faster than conventional CMPC).**

***Index Terms*—Array, model predictive control, wave energy converter.**

I. Introduction

LARGE-CAPACITY and low-cost exploitation of wave energy for grid-scale generation demands forming multiple individual wave energy converters (WECs) into *arrays*, such as the CorPower Ocean's demonstration project HiWave-5 [1]. Under this trend, energy-maximizing control, widely recognized as an effective approach to boosting wave energy capture efficiency [2], faces new challenges. Since a WEC radiates waves outward during its movement, radiation coupling effects exist between any two bodies in a WEC array, making the system hydrodynamics more complicated. Meanwhile, unlike wind farms, the interaction between bodies in a wave farm can be both constructive, or destructive, depending on how their motion is controlled. Currently, the two typical control frameworks for WEC arrays are *decentralized* control, which controls each WEC as an independent device, as shown in Fig. 1(a), and *centralized* (or *coordinated*) control, which controls the entire multi-body system as a whole, as shown in Fig. 1(b). The two frameworks have been compared in a series of simulation studies [3], [4], [5] and experiments [6], [7], and the basic consensus, unsurprisingly, is that centralized control is superior in terms of energy production performance (e.g., 20% improvement [3]), especially when radiation effects are strong (i.e. devices are in relatively close proximity to each other). This superiority is due to the fact that centralized control considers the full system dynamics and is aware of the motion of each device, and can thereby exploit the radiation coupling in a predominantly constructive way. However, compared with single-WEC control that has been intensively studied previously [2], the incorporation of all body movements and radiation effects significantly increases the complexity of coordinately controlling WEC arrays.

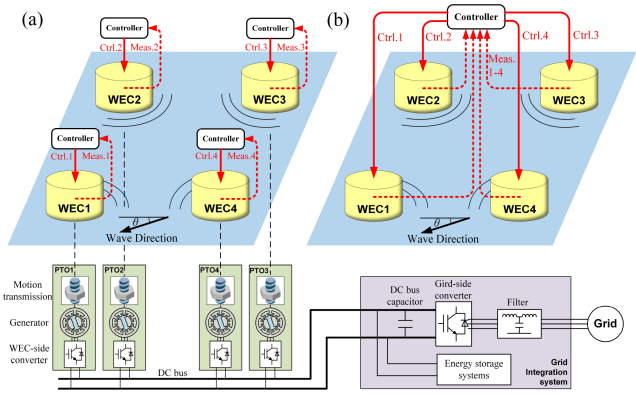

Fig. 1. Schematics of (a) decentralized control and (b) centralized control, with the power take-off (PTO) and grid integration systems. Meas.: measurements. Ctrl.: control command.

Linear control is the simplest controller for WEC arrays, and methods have been developed to derive linear control coefficients by peak-frequency causal approximation [6], and numerical optimization [8], [9]. Latching control is also experimentally examined for a WEC array in [10]. Albeit simple to implement, linear and latching controllers cannot or can only *partially* handle the device safe-operating constraints [8]. Optimal constrained control for WEC arrays is studied using Pontryagin's maximum principle in [11], [12], where the constraints include the limits of power take-off (PTO) force and instantaneous power, and the solution has an analytical, bang-singular-bang form. Also, using Pontryagin's approach, the optimal control

Received 17 September 2024; revised 25 January 2025; accepted 26 February 2025. Date of publication 12 March 2025; date of current version 23 June 2025. This work was supported in part by the National Natural Science Foundation of China under Grant 52337002 and in part by the National Key Research and Development Program of China under Grant 2020YFE0205400. Paper no. TSTE-01166-2024. *(Corresponding Author: Xi Xiao.)*

Zechuan Lin, Xuanrui Huang, Yifei Han, and Xi Xiao are with the Department of Electrical Engineering, Tsinghua University, Beijing 100084, China (e-mail: xiao_xi@tsinghua.edu.cn).

John V. Ringwood is with the Centre for Ocean Energy Research, Maynooth University, Co. Kildare W23 X021, Ireland.

Color versions of one or more figures in this article are available at https://doi.org/10.1109/TSTE.2025.3548931.

Digital Object Identifier 10.1109/TSTE.2025.3548931

trajectory within a maximum displacement is calculated analytically in [13]. Nevertheless, analytical solutions are only attainable for *certain* combinations of constraints. Currently, the state-of-the-art controller for *general* optimal constrained control of WECs is the model predictive control (MPC)-like method [2], which works by numerically optimizing the control moves over a future horizon at each control instant. Note that the simple controllers discussed above are naturally designed 'centrally', namely, targeting total energy production, and do not involve additional computational issues in their implementation, and it is from the numerical-optimization-based MPC that centralization of control raises difficulties in online computation. MPC has been developed for WEC arrays in [3], [5], [14], [15], [16], [17], [18], usually including a centralized (CMPC) with decentralized version (DMPC) for comparison, and CMPC has achieved success in various studies and demonstrated its superior performance. Nevertheless, the computational requirement is growing: Given the well-known fact that the prediction horizon length N_p of MPC needs to be *sufficiently large* to achieve optimal energy capture performance, the optimization dimension of DMPC is N_p, while that of CMPC grows to nN_p, for an n-WEC array. This challenging optimization dimension can make CMPC computationally prohibitive for a real-time controller.

Techniques have been developed to speed up CMPC computation through *parameterization* of the receding-horizon optimal control problem of CMPC, in order to reduce the optimization dimension. Move-blocking is adopted for CMPC in [5], where the control moves during certain steps are held fixed and represented by only one variable. In unconstrained spectral control [4], the system trajectory is represented by a truncated Fourier series. Constrained pseudo-spectral control is further developed [19], where constraints are applied on a series of time points (termed 'collocation points'). Recently proposed moment-based control stands as a more general parameterization approach with better convexity properties [7]. However, as the quality of the control is heavily dependent on the length of the prediction horizon, these methods have focused on *how to approximately solve a long-horizon optimal control problem*, while the requirement for horizon length, as the dominant influencing factor of computational complexity, remains. Another possibility—*how to reduce this requirement*, has been overlooked, which is a new *paradigm* for dimension reduction with great potential.

Another control acceleration strategy, also worth mentioning, is *cooperative* control, developed in [3], [18], [20]. In this method, each WEC is equipped with a local MPC controller, which takes total array energy production as the objective, but only optimizes its own control moves. After obtaining the local solution, the controller transmits it to other controllers; in this way, the overall control problem is solved in an iterative manner. However, the computation acceleration enjoyed by cooperative MPC is rather limited (generally less than 50% as reported in [18]); in contrast, directly shortening the optimization dimension is potentially much more effective.

In this study, a fast CMPC controller for WEC arrays is proposed, based on the idea of *rollout*. In this method, the prediction horizon is kept long, while the optimization horizon is kept short. Only the control moves over the optimization horizon are optimized while, in the remainder of the prediction horizon, the system trajectory is 'rolled out' using a fixed control law, to calculate the total energy production as the objective function. Hence, the optimization dimension can be significantly reduced, while the controller is still aware of future operations, avoiding shortsightedness. Rollout-based MPC has been successfully developed for single WECs [21] and validated through wave tank testing [22], and is here extended to WEC arrays. Specifically, it is proposed to utilize a two-degree-of-freedom (2-DoF) reactive controller as the rollout controller, maintaining limited parameter tuning dimension despite the high-dimensional array model, while being effective in boosting energy generation. A look-up-table-based online tuning strategy is further developed to track the optimal rollout coefficients under *varying sea states*. It will be shown by comprehensive simulations results that the proposed rollout-based CMPC (R-CMPC) can achieve near-optimal energy generation performance across a wide range of sea states, with a significantly lower computational burden than conventional CMPC. In addition, the control sensitivity to non-ideal wave excitation force estimation and forecasting will also be examined.

The remainder of this paper is organized as follows. The modeling of the WEC array is introduced in Section II. Conventional CMPC and DMPC are introduced in Section III. Sea-state-dependent R-CMPC is proposed in Section IV. Simulation results are presented in Section V with conclusions drawn in Section VI.

II. WEC Array Modelling

A. Equation of Motion

In this section, the array model is developed following the widely-used modelling approach of [16]. For a WEC array consisting of n bodies, the equation of motion of the ith body, $i = 1, 2, \ldots, n$, is

$$M^i \ddot{z}^i(t) = f_d^i(t) + f_h^i(t) + f_r^i(t) + w^i(t) + u^i(t), \quad (1)$$

where M^i and $z^i(t)$ are the mass and heave displacement of the ith body, respectively; $f_d^i(t)$ is the linearized viscous force

$$f_d^i(t) = -R_d^i \dot{z}^i(t), \quad (2)$$

where R_d^i is the linearized viscous drag coefficient; $f_h^i(t)$ is the hydrostatic restoring force

$$f_h^i(t) = -K^i z^i(t), \quad (3)$$

where K^i is the hydrostatic stiffness; $f_r^i(t)$ is the radiation force described by

$$f_r^i(t) = \sum_{j=1}^{n} -M_\infty^{ij} \ddot{z}^j(t) - \int_{-\infty}^{t} k_r^{ij}(t-\tau)\dot{z}^j(\tau)\mathrm{d}\tau, \quad (4)$$

where M_∞^{ij} and k_r^{ij} are the infinite-frequency added mass and impulse response function (IRF) of the radiation system of the jth body to the ith body, respectively, with

$$M_\infty^{ij} = \lim_{\omega\to\infty} M_a^{ij}(\omega)$$
$$k_r^{ij}(t) = \frac{2}{\pi}\int_0^\infty R_a^{ij}(\omega)\cos(\omega t)\mathrm{d}\omega, \quad (5)$$

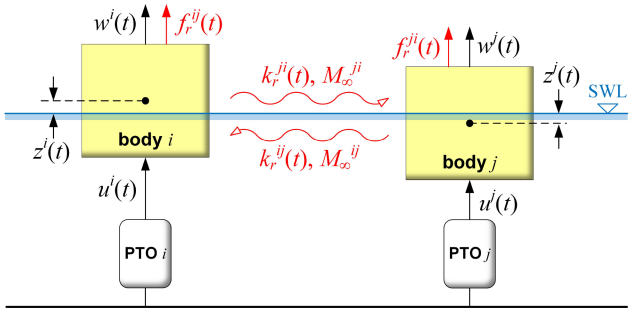

Fig. 2. Diagram of the hydrodynamic system between the ith and jth bodies. Note that $k_r^{ij} = k_r^{ji}$ and $M_\infty^{ij} = M_\infty^{ji}$. SWL: Still water level.

where ω is angular frequency, and $M_a^{ij}(\omega)$ and $R_a^{ij}(\omega)$ are the frequency-domain added mass and damping of the mutual radiation system. Finally, $w^i(t)$ and $u^i(t)$ are the wave excitation force and PTO force on the ith body, respectively. An illustration of the hydrodynamic system is given in Fig. 2.

B. State-Space Model

To develop an overall state-space model, the radiation forces in (4) are approximated by state-space models

$$\begin{aligned} \dot{\zeta}^{ij}(t) &= A_r^{ij}\zeta^{ij}(t) + B_r^{ij}\dot{z}^j(t) \\ \int_{-\infty}^{t} k_r^{ij}(t-\tau)\dot{z}^j(\tau)\mathrm{d}\tau &\approx C_r^{ij}\zeta^{ij}(t), \end{aligned} \tag{6}$$

where $\zeta^{ij}(t) \in \mathbb{R}^{l^{ij}}$ is the l^{ij}-dimensional state vector of this subsystem, and $A_r^{ij} \in \mathbb{R}^{l^{ij}\times l^{ij}}$, $B_r^{ij} \in \mathbb{R}^{l^{ij}\times 1}$, and $C_r^{ij} \in \mathbb{R}^{1\times l^{ij}}$ are the associated matrices. This approximation can be achieved using system identification techniques (e.g., [23]). Note that a n-body array has n^2 radiation subsystems.

Based on (6), the state-space model of the WEC array can be written as

$$\begin{aligned} \dot{x}(t) &= A_c x(t) + B_c(u(t) + w(t)) \\ y(t) &= Cx(t), \end{aligned} \tag{7}$$

where $x(t)$ is the overall state, $y(t)$ is the measurable state consisting of the velocities and positions of all bodies, and $w(t)$ and $u(t)$ are the wave excitation force and PTO force vectors, respectively:

$$\begin{aligned} x &= [\dot{z}^{\mathrm{T}}, z^{\mathrm{T}}, \zeta^{11,\mathrm{T}}, \ldots, \zeta^{1n,\mathrm{T}}, \ldots, \zeta^{nn,\mathrm{T}}]^{\mathrm{T}} \\ y &= [\dot{z}^{\mathrm{T}}, z^{\mathrm{T}}]^{\mathrm{T}} \\ z &= [z^1, z^2, \ldots, z^n]^{\mathrm{T}} \\ u &= [u^1, u^2, \ldots, u^n]^{\mathrm{T}} \\ w &= [w^1, w^2, \ldots, w^n]^{\mathrm{T}}, \end{aligned} \tag{8}$$

where $z, u, w \in \mathbb{R}^n$; $y \in \mathbb{R}^{2n}$; let $l = \sum_{i=1}^{n}\sum_{j=1}^{n} l^{ij}$, and $x \in \mathbb{R}^m$ with $m = 2n + l$; A_c, B_c, and C are the associated matrices

$$A_c = \begin{bmatrix} -M^{-1}R & -M^{-1}K & -M^{-1}C_r \\ \mathbf{I}_n & \mathbf{0}_{n\times n} & \mathbf{0}_{n\times l} \\ B_r & \mathbf{0}_{l\times n} & A_r \end{bmatrix}, B_c = \begin{bmatrix} M^{-1} \\ \mathbf{0}_{n\times n} \\ \mathbf{0}_{l\times n} \end{bmatrix}$$

$$C = \begin{bmatrix} \mathbf{I}_n & \mathbf{0}_{n\times n} & \mathbf{0}_{n\times l} \\ \mathbf{0}_{n\times n} & \mathbf{I}_n & \mathbf{0}_{n\times l} \end{bmatrix}, \tag{9}$$

where $\mathbf{I}_n$ denotes an n-dimensional identity matrix, $\mathbf{0}_{n\times l}$ denotes an $n \times l$ zero matrix, and

$$\begin{aligned} M &= \mathrm{diag}(M^1, M^2, \ldots, M^n) + [M_\infty^{ij}] \\ R &= \mathrm{diag}(R_d^1, R_d^2, \ldots, R_d^n) \\ K &= \mathrm{diag}(K^1, K^2, \ldots, K^n) \\ A_r &= \mathrm{blkdiag}(A_r^{11}, \ldots, A_r^{1n}, \ldots, A_r^{nn}) \\ B_r &= [B_r^{1,\mathrm{T}}, B_r^{2,\mathrm{T}}, \ldots, B_r^{n,\mathrm{T}}]^{\mathrm{T}} \\ B_r^i &= \mathrm{blkdiag}(B_r^{i1}, B_r^{i2}, \ldots, B_r^{in}), \quad i = 1, 2, \ldots, n \\ C_r &= \mathrm{blkdiag}(C_r^1, C_r^2, \ldots, C_r^n) \\ C_r^i &= [C_r^{i1}, C_r^{i2}, \ldots, C_r^{in}], \quad i = 1, 2, \ldots, n, \end{aligned} \tag{10}$$

with $A_c \in \mathbb{R}^{m\times m}$, $B_c \in \mathbb{R}^{m\times n}$, $C \in \mathbb{R}^{2n\times m}$, $M, K, R \in \mathbb{R}^{n\times n}$, $A_r \in \mathbb{R}^{l\times l}$, $B_r \in \mathbb{R}^{l\times n}$, and $C_r \in \mathbb{R}^{n\times l}$.

III. Conventional MPC for WEC Arrays

The WEC array control task is to determine the optimal PTO force $u^i(t), i = 1, \ldots, n$ for each body, such that the long-term power production, represented by

$$P = \lim_{T_f\to\infty} \frac{1}{T_f}\int_0^{T_f} -\sum_{i=1}^{n} \dot{z}^i(t)u^i(t)\mathrm{d}t, \tag{11}$$

is maximized, while respecting individual device constraints. Note that this study focuses on the array control complexity issue by considering only mechanical energy production (11). However, the control can be extended to account for electrical efficiency by incorporating quadratic loss functions as in [24], [25].

A. Conventional CMPC and DMPC Formulations

MPC-like controllers are recognized as the state-of-the-art solution for constrained optimal control of WECs [2]. To begin with, the continuous model may be discretized as

$$\begin{aligned} x_{k+1} &= Ax_k + B(u_k + w_k) \\ y_k &= Cx_k, \end{aligned} \tag{12}$$

where k is the discrete time index with a sampling period of T_s, and matrices A and B can be obtained from A_c and B_c using zero-order hold equivalents as $A = \exp(A_c T_s)$ and $B = \int_0^{T_s} \exp(A_c\tau)\mathrm{d}\tau B_c$. Note that, while it is also possible to use first-order-hold discretization, zero-order-hold is adopted here, due to its simplicity and sufficiently good performance [13]. Define $C_1 = [\mathbf{I}_n, \mathbf{0}_{n\times n}, \mathbf{0}_{n\times l}]$ and $C_2 = [\mathbf{0}_{n\times n}, \mathbf{I}_n, \mathbf{0}_{n\times l}]$, so that $C_1 x_k = \dot{z}_k$ and $C_2 x_k = z_k$. The one-step energy output of the array can be calculated, using the trapezoidal rule of integration, as

$$\begin{aligned} E_k &\approx -\sum_{i=1}^{n} \frac{T_s}{2}(\dot{z}_k^i + \dot{z}_{k+1}^i)u_k^i \\ &= -\frac{T_s}{2}(C_1 x_k + C_1 x_{k+1})^{\mathrm{T}} u_k. \end{aligned} \tag{13}$$

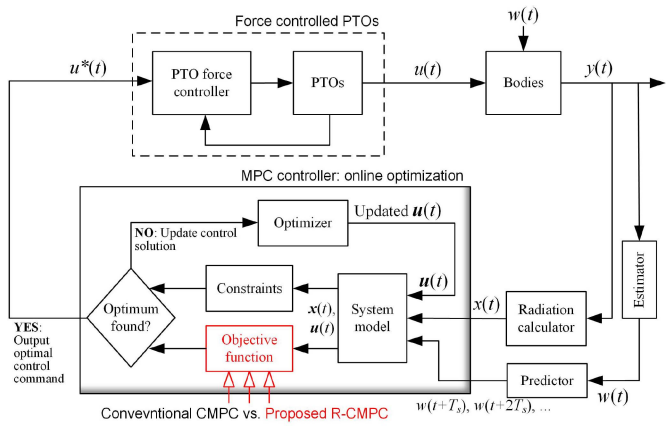

Fig. 3. Control diagram of CMPC. The studied controller is the MPC controller, which outputs an optimal PTO force command $u^*(t)$. The force command is then tracked by a PTO controller, which can be achieved by mature electrical machine control technologies [24]. The estimator and predictor are described in Section III-B. The innovation of this paper targets the objective function (red part) of CMPC.

The constraints typically include the maximum displacement and maximum PTO force of each WEC body, expressed as

$$|C_2 x_k| \le Z_m, \quad |u_k| \le U_m. \tag{14}$$

MPC for WECs adopts a finite-horizon energy-maximizing problem formulation, where at each step: i) The current system state x_k is observed; ii) the future wave excitation force is predicted for N_p steps as w_k, w_{k+1},..., w_{k+N_p-1}, with N_p the *prediction horizon*; iii) based on i) and ii), for any N_p-step control sequence u_k, u_{k+1},..., u_{k+N_p-1}, the future system trajectory x_{k+1}, x_{k+2},..., x_{k+N_p}, as well as the energy production E_k, E_{k+1},..., E_{k+N_p-1}, can be calculated by iteratively using (12) and (13); hence, iv) an optimal N_p-step control sequence is solved, such that it maximizes $E = \sum_{i=0}^{N_p-1} E_{k+i}$, while keeping the controls u_k, u_{k+1},..., u_{k+N_p-1} and states x_{k+1}, x_{k+2},..., x_{k+N_p} within the corresponding constraints (14); finally, v) only the first control move u_k is applied to the system. The above process is illustrated in Fig. 3. Specifically, the MPC optimal control problem can be summarized as

$$\begin{aligned} \max_{\mathbf{u}_k} \quad & E = -\sum_{i=0}^{N_p-1} \frac{T_s}{2}(C_1 x_{k+i} + C_1 x_{k+i+1})^{\mathrm{T}} u_{k+i} \\ \text{s.t.} \quad & x_{k+i+1} = A x_{k+i} + B(u_{k+i} + w_{k+i}), \\ & \qquad\qquad i = 0, \ldots, N_p - 1 \\ & |C_2 x_{k+i+1}| \le Z_m, \quad |u_{k+i}| \le U_m, \\ & \qquad\qquad i = 0, \ldots, N_p - 1, \end{aligned} \tag{15}$$

where $\mathbf{u}_k = [u_k^{\mathrm{T}}, u_{k+1}^{\mathrm{T}}, \ldots, u_{k+N_p-1}^{\mathrm{T}}]^{\mathrm{T}} \in \mathbb{R}^{nN_p}$ is the control sequence over the prediction horizon, as the optimization variable. It is easy to verify that this is a parametric quadratic program (QP), whose derivation is similar to [21]. Note that the MPC problem dimension nN_p is not related to the system model dimension m, since a 'dense' formulation is adopted, with all the future system states dependent on $\mathbf{u}_k$ rather than being treated as separated variables [21]. Problem (15), using the overall system model (12) and optimizing all control moves together, corresponds to the conventional CMPC and leads to *one* central controller, as shown in Fig. 1(b).

However, since problem (15) needs to be repeatedly solved in real time, the main challenge in its application is the online computational burden. It is well known that MPC for WECs requires a sufficiently long prediction horizon N_p to achieve optimal energy production performance. Meanwhile, conventionally in WEC MPC, no distinction is made between the prediction horizon N_p, over which the system trajectory is predicted, and the *optimization horizon* N_o, over which the control sequence is optimized (this distinction will play a central role in the fast MPC to be proposed later). Hence, for conventional CMPC, N_o *equals* N_p and is generally a large value. Consequently, this leads to a large optimization dimension for MPC for a *single* WEC, which is N_p, and a further *increased* dimension for CMPC for WEC *arrays*, which is nN_p, leading to a potentially prohibitive computational load.

A straightforward approach to reducing the computational burden is to treat each body of the array as an independent body by neglecting all mutual radiation. This *decentralized* MPC (DMPC) leads to n separate controllers, each with an optimization dimension of N_p and without communication requirements, as shown in Fig. 1(a). DMPC for each WEC can be derived similarly to CMPC, which can be regarded as a special case of $n = 1$. However, since mutual radiation effects are ignored, such decentralized control will lead to degradation of energy capture performance [3], [4], [5], [6], [7].

B. MPC Requirements: State Observation, Wave Excitation Force Estimation, and Forecast

Control optimization of MPC requires full state observation and wave excitation force information, which are detailed as follows:

1) For state observation, all the radiation subsystem states ζ_k^{ij} can be directly calculated from the measurable $\dot{z}_k$ and (a discrete realization of) (6).
2) The wave excitation force is not directly measurable, and an established approach is estimating w_k as an unknown input using the system model and available measurements. This estimation problem, in WEC applications, has been intensively studied [26], and this paper adopts the technique based on a Kalman filter (KF) with a random-walk model, which is sufficient to achieve good accuracy, provided that the model is correct [26]. For centralized controllers, a *global* KF-based estimator, i.e., one that estimates w for all bodies, using the overall model (12) and the measurements from all bodies, is employed. For decentralized controllers, in addition, *independent* estimators that estimate w for each body, using a single-body model and the measurements from that body alone, are examined. Note that, since each independent estimator is not aware of the motion of other bodies, it cannot distinguish between incident wave excitation forces and mutual radiation forces [27].

3) Once the instantaneous w_k is obtained, the future values of w can be predicted from its past values using time-series models. This paper will adopt a linear direct multi-step (DMS) model, which can be easily identified from time series data and can achieve close-to-optimal accuracy [28]. For centralized controllers, a *global* DMS forecaster, i.e., one that forecasts using the w information of *all* bodies, is employed. For decentralized controllers, in addition, *independent* forecasters that predict w for each body only using the w information of that body, are also examined. Note that, for the global forecaster, information from up-wave bodies can be utilized to improve the forecasting accuracy of down-wave bodies, so the overall accuracy is naturally higher than independent forecasters.

The above components are shown in Fig. 3. This paper is focused on the CMPC (control) algorithm and will not delve into the details of the WEC array estimation-forecast problem. However, the non-ideal estimation and forecasting described above are used to study the control sensitivity in Section V-F.

IV. Sea-State-Dependent Rollout-Based CMPC

A. Rollout-Based CMPC

As mentioned earlier, N_o in conventional CMPC always equals N_p, and it is this *coupling* between N_o and N_p that results in the high optimization dimension. Hence, it is worthwhile to study how to *decouple* N_o and N_p; specifically, let $N_o < N_p$, in order to maintain long-horizon prediction with short-horizon optimization. Such a decoupling is, in fact, a natural development of traditional MPC [29]. For WEC application, the *rollout* method, widely used in artificial intelligence systems (e.g., [30]) and applied for single WECs in [21], [22], is adopted here. The basic idea of rollout-based MPC is to only optimize a few control moves (a small N_o) assuming that, for the remaining $N_r = N_p - N_o$ steps of the prediction horizon (a large N_p), the system will be controlled by a fixed control law; N_r is termed the rollout horizon. Rolling out the remaining horizon with a pre-determined control law, rather than fully expanding those control possibilities, can incorporate future information into the short-horizon planning, without increasing the computational burden.

Let $u_k = \mu(x_k)$ be the general-form state-feedback control law for rollout; then rollout-based CMPC (R-CMPC) corresponds to the following optimal control problem:

$$\begin{aligned}\max_{\mathbf{u}_k} \quad & E = -\sum_{i=0}^{N_o-1} \frac{T_s}{2}(C_1x_{k+i} + C_1x_{k+i+1})^{\mathrm{T}}u_{k+i} \\ & \quad -\sum_{i=N_o}^{N_p-1} \frac{T_s}{2}(C_1x_{k+i} + C_1x_{k+i+1})^{\mathrm{T}}u_{k+i} \\ \text{s.t.} \quad & x_{k+i+1} = Ax_{k+i} + B(u_{k+i} + w_{k+i}), \\ & \qquad i = 0, \ldots, N_o - 1 \\ & |C_2x_{k+i+1}| \le Z_m, \quad |u_{k+i}| \le U_m, \\ & \qquad i = 0, \ldots, N_o - 1\end{aligned}$$

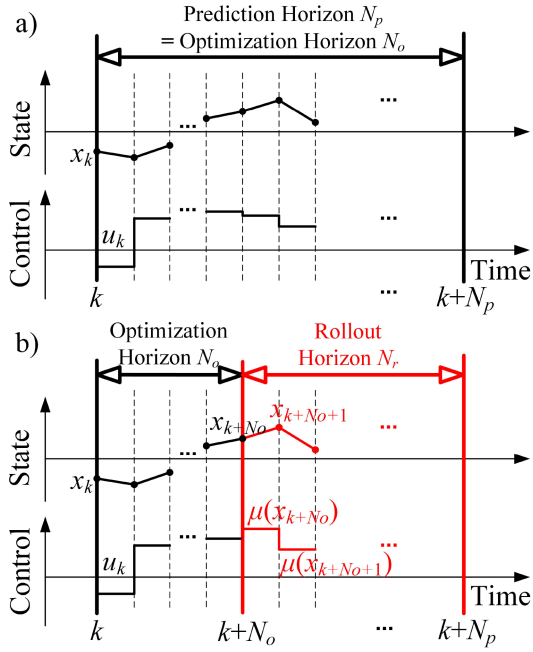

Fig. 4. Illustrations of a) the conventional CMPC and b) rollout-based MPC.

$$\begin{aligned}x_{k+i+1} &= Ax_{k+i} + B(\mu(x_{k+i}) + w_{k+i}), \\ & \qquad i = N_o, \ldots, N_p - 1 \qquad (16)\end{aligned}$$

where $\mathbf{u}_k = [u_k^{\mathrm{T}}, u_{k+1}^{\mathrm{T}}, \ldots, u_{k+N_o-1}^{\mathrm{T}}]^{\mathrm{T}} \in \mathbb{R}^{nN_o}$ is the control sequence consisting of the first N_o moves only. A rollout trajectory beyond N_o steps is calculated using controller $\mu(\cdot)$, and the generated energy is included in the objective function. A comparison of conventional CMPC (15) and R-CMPC (16) is illustrated in Fig. 4, highlighting the difference in the control horizon. Note that the constraints corresponding to Z_m and U_m are also applied only on the first N_o moves, so the number of constraints also decreases.

To better understand the rollout technique, define the following function

$$\begin{aligned}V_\mu(x_{k+N_o}, \mathbf{w}_{f,k}) = & -\sum_{i=N_o}^{N_p-1} \frac{T_s}{2}(C_1x_{k+i} + C_1x_{k+i+1})^{\mathrm{T}}u_{k+i} \\ \text{s.t.} \quad & x_{k+i+1} = Ax_{k+i} + B(\mu(x_{k+i}) + w_{k+i}), \\ & \qquad i = N_o, \ldots, N_p - 1, \quad (17)\end{aligned}$$

which represents the generated energy when the system starts from x_{k+N_o}, is controlled by $\mu(\cdot)$, and experiences WEF sequence $\mathbf{w}_{f,k} = [w_{k+N_o}^{\mathrm{T}}, \ldots, w_{k+N_p-1}^{\mathrm{T}}]^{\mathrm{T}}$. With (17), R-CMPC problem (16) can now be expressed as

$$\begin{aligned}\max_{\mathbf{u}_k} \quad & E = -\sum_{i=0}^{N_o-1} \frac{T_s}{2}(C_1x_{k+i} + C_1x_{k+i+1})^{\mathrm{T}}u_{k+i} \\ & \qquad + V_\mu(x_{k+N_o}, \mathbf{w}_{f,k}) \\ \text{s.t.} \quad & x_{k+i+1} = Ax_{k+i} + B(u_{k+i} + w_{k+i}), \\ & \qquad i = 0, \ldots, N_o - 1\end{aligned}$$

$$|C_2 x_{k+i+1}| \le Z_m, \quad |u_{k+i}| \le U_m, \quad i = 0, \ldots, N_o - 1. \tag{18}$$

Comparing (18) with (15), it is now clear that, essentially, R-CMPC adds a *terminal value function*, i.e. (17), to conventional CMPC (where $N_o = N_p$). This equivalence is also highlighted in [21] for a single WEC. Note that (17) is a function of the terminal state *and* the future wave excitation forces $\mathbf{w}_{f,k}$.

B. The Choice of Rollout Controller $\mu(x_k)$

The performance of R-CMPC relies heavily on the choice of the rollout controller $\mu(x_k)$, especially when a small N_o is needed. Important considerations in making the choice of the rollout controller are:

1) In order to maintain problem (16) as a QP, rather than a nonlinear program, it is desirable to use a *linear* feedback controller to roll out the system, namely,
$$\mu(x_k) = \Phi x_k, \tag{19}$$
where $\Phi \in \mathbb{R}^{n \times m}$ is the control coefficient (matrix).
2) There is *no* direct relationship between the energy capture performance of $\mu(x_k)$ itself and that of the R-CMPC using $\mu(x_k)$ for rollout. A 'policy improvement theorem' is revealed in [21] guaranteeing that, under certain conditions (e.g., unconstrained), the performance of R-CMPC is not worse than $\mu(x_k)$. But, in general, the best controller for controlling the WEC is *not necessarily* the best choice for rollout. [21]. The rollout controller serves, rather, as a 'heuristic' guess, and its efficacy can only be evaluated in terms of the performance of R-CMPC.
3) Since the performance of linear feedback control is affected by the sea state, which is typically characterized by significant wave height H_s and peak period T_p, the R-CMPC performance may also have certain *sea-state dependence*, as will be shown in the next section. Consequently, like the linear control itself, the rollout control coefficients Φ of R-CMPC need to be tuned online, according to the varying sea state.
4) An online tuning strategy discussed in 3) is technically mature to implement. The sea state can be estimated from the WEC motion through an estimator [31] or from meteorological office forecasts. As a relatively long-term parameter, sea state estimation only needs to be updated at an infrequent rate (e.g., once every 20 minutes). The only outstanding unknown, through offline simulation of R-CMPC, is the optimal Φ for each sea state; after that, the optimal coefficients can be stored in a look-up table for online use.
5) Since simulation of MPC-like controllers is computationally intensive, it is impossible to expand all possibilities of the high-dimensional $\Phi \in \mathbb{R}^{n \times m}$ to find the optimal parameters for each sea state. The number of degrees of freedom (DoF) of Φ needs to be suitably restricted.

Summarizing the above, it is proposed to use a linear feedback reactive control as the rollout control law

$$u_k^i = R_g^i \dot{z}_k^i + K_g^i z_k^i, \quad i = 1, \ldots, n, \tag{20}$$

where R_g^i and K_g^i are the PTO damping and stiffness of the ith body, as the reactive control coefficients. Note that the control force of each body depends only on its own motion and not on the self- or mutual-radiation states; such control is also adopted for WEC arrays in [9]. Combining (19) and (20), the rollout control matrix is

$$\Phi = \begin{bmatrix} R_g, & K_g, & \mathbf{0}_{n \times l} \end{bmatrix}, \tag{21}$$

where

$$R_g = \mathrm{diag}(R_g^1, \ldots, R_g^n)$$
$$K_g = \mathrm{diag}(K_g^1, \ldots, K_g^n). \tag{22}$$

Meanwhile, since currently almost all WEC array deployments are *homogeneous*, namely, all bodies are identical (note that *heterogeneous* array is a concept that has only been studied very recently [11] and is still under development), let all bodies share the same rollout coefficients $\bar{R}_g$ and $\bar{K}_g$, namely,

$$R_g^1 = R_g^2 = \ldots = R_g^n = \bar{R}_g$$
$$K_g^1 = K_g^2 = \ldots = K_g^n = \bar{K}_g, \tag{23}$$

then the DoF count of the rollout controller is reduced to 2, allowing for an easy coefficient-searching process. Using H_s and T_p to describe the sea state, the sea-state dependence of the rollout coefficients can be expressed as

$$\bar{R}_g = \bar{R}_g(H_s, T_p)$$
$$\bar{K}_g = \bar{K}_g(H_s, T_p), \tag{24}$$

and the optimal mappings are calculated offline to form a look-up table. Note that another sea state parameter, the wave direction θ, does not affect the optimal coefficients, as will be shown in the next section. This provides convenience for offline coefficient tuning and also for online implementation, since real-time identification of wave direction is not needed. Finally, the QP formulation can be derived similarly to [21].

Conventional CMPC (15), although without a theoretical guarantee, is typically convex or at least can be convexified by penalty terms [15]. As discussed in Section IV-A, R-CMPC (16) can be viewed as adding a terminal value function to conventional CMPC. Crucially, such a terminal value function, based on a reactive (rollout) controller, is typically convex. To see this, one can look at the previous study on rollout-based MPC for a single WEC [21], where a detailed quadratic program derivation is presented. According to (16) and (17) in [21], the convexity of the terminal value function depends on $\mathbf{H_f}$, and eventually on $\mathbf{H_{xx}}$. According to (13) in [21], the physical meaning of $x^{\mathrm{T}}\mathbf{H_{xx}}x$ is the energy generation by a reactive controller, when the system starts from initial state x with *no* wave excitation. Since the reactive control coefficients are selected from a reasonable range (e.g., avoiding instability) and the rollout horizon is selected sufficiently long (this will be discussed in Section V-C), the device will undergo a free-decay process, and the final extracted energy by the reactive controller is positive. Hence, $\mathbf{H_{xx}}$ is positive definite, and $\mathbf{H_f}$ is at least positive semi-definite. This result can be easily extended to the WEC array case in this study. Hence, the rollout technique can

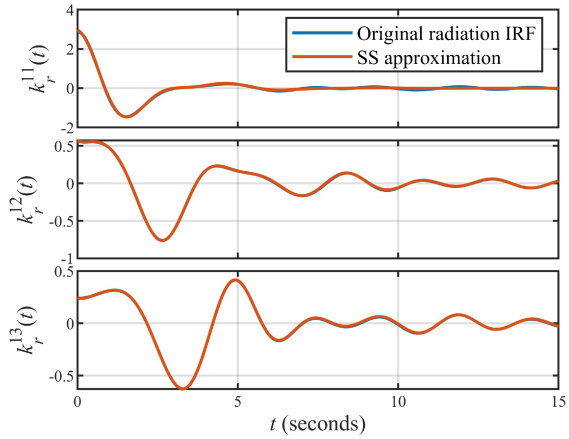

Fig. 5. The radiation IRFs and their SS approximations.

help *convexify* the MPC problem, which is another desirable feature.

V. Results

A. Case Study Setup

The studied case is a 2 × 2 cylinder WEC array as shown in Fig. 1. Each body has a radius of 1.5 m and a draught of 1.5 m, and the bodies are arranged in a square with a side length of 8 m. The hydrodynamic model parameters are computed using Capytaine [32]. Due to the symmetry of the array layout, there exist three unique radiation IRFs, namely $k_r^{11}(t)$, $k_r^{12}(t)$, and $k_r^{13}(t)$. The corresponding state-space (SS) models are identified using [23], based on an improved Prony method, with dimensions $l^{11} = 4$, $l^{12} = 8$, and $l^{13} = 10$, respectively, selected to be necessarily large to achieve good accuracy. The IRFs and SS approximations are shown in Fig. 5, from which the 'time delay' effects in mutual radiation forces can be partially observed. The total radiation state dimension is $l = 120$. The viscous force coefficient is calculated following [33] and linearized at $\dot{z} = 0.5$ m/s, yielding $R_d = 1.77$ kN/(m/s). The maximum displacement Z_m is 1.5 m, equal to the draught, and the maximum PTO force is $U_m = 60$ kN.

The studied sea state ranges from $H_s = 0.5$ m–1.4 m and $T_p = 4$ s–7 s, which is selected to cover the main wave energy generation range of a real ocean dataset [24]. The wave direction θ is considered independently of H_s and T_p; due to the symmetric square arrangement, only the $\theta \in [0°, 45°]$ range needs to be considered, with the 0° direction defined as in Fig. 1. For each sea state, the waves are modeled using the Bretschneider spectrum and then simulated in the time domain, to evaluate the control performance. Until Section V-F, the wave excitation force information will be assumed ideal.

B. Control Example

First, an example to illustrate the efficacy of R-CMPC is presented. The sea state is $H_s = 1.1$ m and $T_p = 6.0$ s with a wave direction $\theta = 30°$, and the following controllers are compared: i) A conventional CMPC with $T_s = 0.25$ s and a sufficiently long

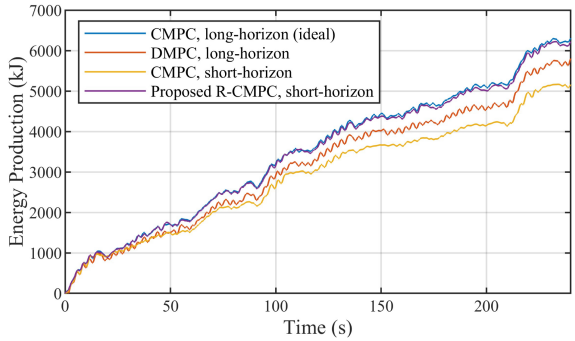

(a) Total energy production of the array. R3C4

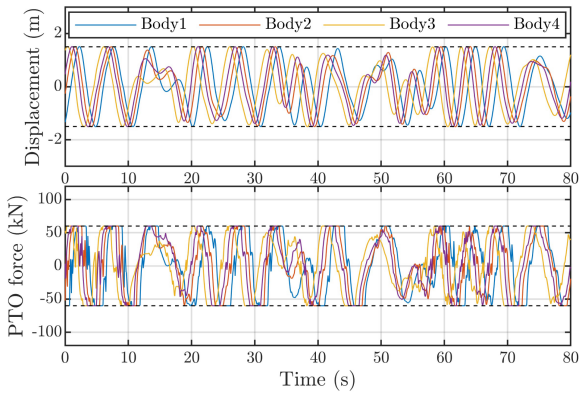

(b) Control trajectory of R-CMPC.

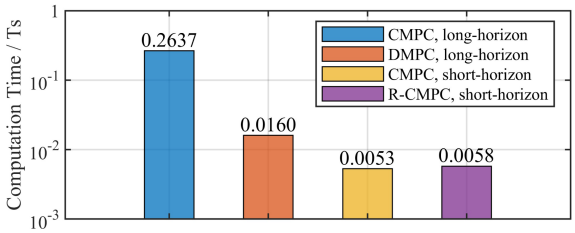

(c) Average control computation time in simulation, as a fraction of the sampling period T_s=0.25 s. R3C5

Fig. 6. An illustrative comparison of the four controllers.

prediction/optimization horizon of $N_o = N_p = 36$, representing the ideal case, ii) a DMPC with the same $N_o = N_p = 36$, iii) a conventional CMPC with short horizons of $N_o = N_p = 6$, representing a *realistic* case when the computational power is limited, and iv) the proposed R-CMPC with the same, short, optimization horizon of $N_o = 6$, while other parameters are $N_p = 46$, $\bar{R}_g = -20$ kN/(m/s), and $\bar{K}_g = 40$ kN/m, whose determination will be discussed later. Simulation results are shown in Fig. 6. The simulation is conducted in the MATLAB environment on an Intel i7-13700H platform, where the QPs of MPC are solved using the 'quadprog' function based on an interior-point method [34], and the average computation time is recorded.

It can be observed from Fig. 6(a) that the ideal, long-horizon, CMPC achieves the highest energy production whereas, not surprisingly, DMPC leads to about 8% energy degradation, due to its ignorance of mutual radiation effects. However, the ideal CMPC requires online optimization with a high dimension

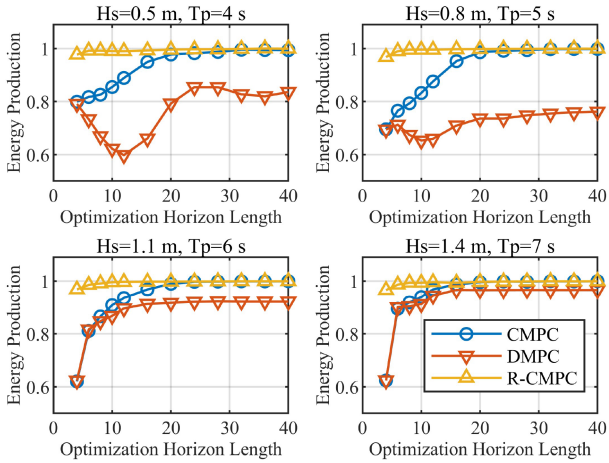

Fig. 7. Relationship between N_o and energy production performance (normalized against the ideal CMPC) of different controllers.

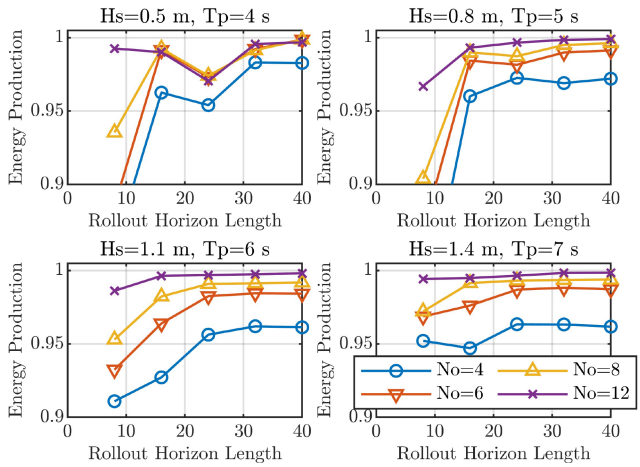

Fig. 8. Relationship between N_r and energy production performance (normalized against the ideal CMPC) of R-CMPC.

$(4 \times 36 = 144$ in this case). When the computational power is limited, conventional CMPC may have to reduce its optimization horizon, and a short-horizon CMPC with a lower dimension $(4 \times 6 = 24$ in this case) can lead to a performance decrease of 20%. In comparison, the proposed R-CMPC maintains the short optimization horizon but achieves over 99% of the energy produced by an ideal CMPC. Crucially, all WECs are properly driven within the constraints, as shown in Fig. 6(b), which verifies that applying constraints only over a short horizon suffices to maintain constraint satisfaction in closed-loop operation. Hence, R-CMPC can reach almost the same control performance as ideal CMPC with a significantly lower optimization dimension (*one-sixth* of ideal CMPC). This reduction in dimension leads to a computational acceleration by a factor of 40, as shown in Fig. 6(c). Also note that R-CMPC is also faster than DMPC, whose dimension is 36; the only advantage of DMPC over R-CMPC is that no communication is required. In addition, note that the comparison against T_s in Fig. 6(c) is only for reference and does not guarantee real-time applicability. Real-time embedded controllers (e.g. DSPs) typically have much lower computational force than PCs [25], under which the implementation of full-horizon CMPC will be a significant challenge.

C. Choice of Optimization and Rollout Horizons

The selection of MPC horizons is now detailed. As a basis, the samping period for MPC prediction is set to $T_s = 0.25$ s, which strikes a balance between the number of control moves for a given prediction (time) horizon while avoiding performance degradation due to discretization error. The impact of N_o $(=N_p)$ of conventional CMPC is shown in Fig. 7 (blue curves) under four different (increasing) sea states. A typical trend of increasing energy performance with increasing N_o is observed and, in order to reach optimal performance, N_o needs to be sufficiently large. It can be seen that the *minimal* N_o required for optimality varies with the sea state, with lesser sea states tending to demand a larger N_o. Considering the preponderance of these factors, $N_o = 36$ is determined as ideal for conventional CMPC, for all the considered sea states. In addition, DMPC performance also increases with N_o, although the performance limits are suboptimal, as shown in Fig. 7 (red curves). Also, note that the suboptimality of DMPC is more significant with lesser energetic sea states.

For R-CMPC, the rollout horizon is set to $N_r = 40$ (to be discussed later), and the performance/N_o relationship $(N_p = N_o{+}N_r)$ is shown in Fig. 7 (yellow curves). It can be seen that R-CMPC performs consistently higher than conventional CMPC, and this superiority is most significant for a small N_o. With $N_o = 6$, R-CMPC is capable of reaching near-optimal energy production, while conventional CMPC can lead to 25% energy waste. Hence, $N_o = 6$ is determined for R-CMPC for all considered sea states. This very small optimization dimension requirement is the central advantage of R-CMPC.

The impact of N_r, under different N_o, for R-CMPC is further shown in Fig. 8, where the best performance is always reached when N_r is sufficiently large. This is because a longer rollout horizon can incorporate more information on future operations, thereby improving the quality of MPC planning. Also note that performance does not increase monotonically with N_r, which can be partially explained by the 'policy improvement theorem' in [21], which requires a large N_r to reach a 'steady-state trajectory', in order to ensure a stable performance-improving effect. In contrast to the fact that N_o determines the performance-computation tradeoff, the impact of N_r on the computational load is *negligible* compared to N_o, since instead of the QP dimension, N_r only affects the calculation of the QP parameters [21]. Hence, N_r can be large enough to reach the performance limit, and $N_r = 40$ suffices for this standard.

D. Impact of Reactive Control Coefficients for Rollout

The above results of R-CMPC are based on the optimal rollout coefficients $\bar{R}_g$ and $\bar{K}_g$, whose selection is now detailed. For each sea state, different values for $\bar{R}_g$ and $\bar{K}_g$ are used for R-CMPC, whose energy production is then simulated. This test is performed for a wide range of sea states described by varying H_s and T_p, with results shown in Fig. 9. It can be seen that, first of all, the relationship between energy production and rollout

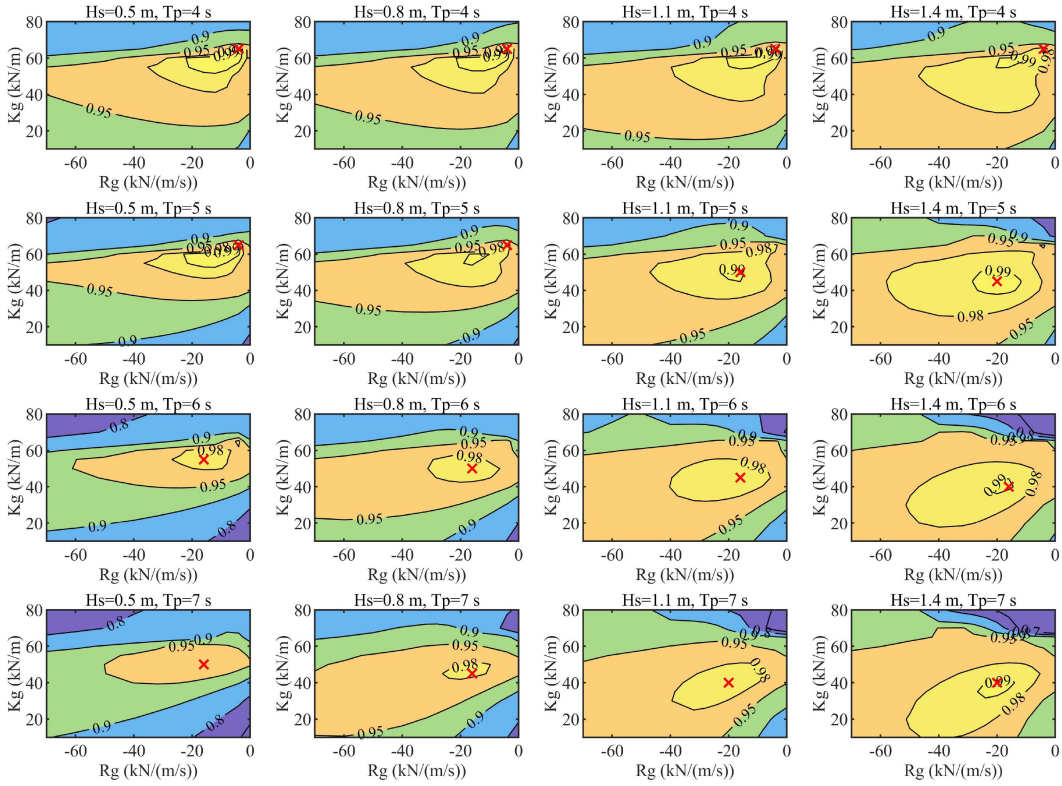

Fig. 9. R-CMPC energy production performance (normalized against the ideal CMPC) with different rollout coefficients.

coefficients is different under different sea states. Under all sea states, there exists a unique $(\bar{R}_g, \bar{K}_g)$ pair for R-CMPC to reach greatest energy production, as marked with red crosses in Fig. 9, and this limit is typically more than 98% of the ideal CMPC (sometimes very close to 100%); this verifies the efficacy of R-CMPC. Meanwhile, the suboptimal $(\bar{R}_g, \bar{K}_g)$ region with energy production over 95% of the optimum, termed the '95% suboptimal region', is rather large; this shows a certain degree of control *insensitivity* to rollout coefficients. On the other hand, if inappropriate coefficients are selected, R-CMPC performance can decrease significantly. In addition, it is verified that the quadratic program obtained from R-CMPC remains convex, as for conventional CMPC.

Fig. 9 gives instructions to the choice of $\bar{R}_g$ and $\bar{K}_g$ for R-CMPC. First, the control insensitivity to rollout coefficients under all sea states, in turn, corresponds to control insensitivity to *sea states* with a fixed set of rollout coefficients. For example, it is possible to find the overlapping area of the 97% suboptimal regions and pick an $(\bar{R}_g, \bar{K}_g)$ pair from this region, so they can be held fixed under varying sea states; this strategy is adopted in [21]. However, it is more profitable to adjust $\bar{R}_g$ and $\bar{K}_g$ according to the sea state, in order to maximize the energy production. Since no theoretical relationship between the optimal coefficients and sea state can be obtained as in classical reactive control, this sea-state dependence necessitates the use of a look-up-table-based online tuning strategy, which requires some offline pre-simulation and online sea state observation, but does not add additional online computation complexity to CMPC. Additionally, two observations are worth mentioning:

TABLE I
OPTIMAL ROLLOUT COEFFICIENTS UNDER DIFFERENT WAVE DIRECTIONS ($H_s = 1.1$ M, $T_p = 6$ S)

	θ=0°	θ=15°	θ=30°	θ=45°
Optimal $\bar{R}_g$ (kN/(m/s))	-16	-16	-16	-16
Optimal $\bar{K}_g$ (kN/m)	45	45	45	45
Power Production (kW)	26.55	26.65	26.85	26.96

i) From left to right of Fig. 9, as H_s increases, the 98% suboptimal region enlarges, while ii) from top to bottom, as T_p increases, the change trend of this region is not fixed. This may indicate that R-CMPC performance is less sensitive to $\bar{R}_g$ and $\bar{K}_g$ under *tighter* constraints, which mainly occurs when H_s is large.

In addition to H_s and T_p, simulation has indicated that the wave direction θ is almost irrelevant to the *relative* performance of MPCs, compared to the ideal CMPC. The R-CMPC coefficient search results under $\theta = 0°$, $15°$, $30°$, and $45°$ are shown in Table I, and one can observe identical optimal rollout coefficients. Similar conclusions can be drawn from the studies on MPC horizons in Section V-C. Hence, all MPC parameters (e.g., N_o, N_r, $\bar{R}_g$, and $\bar{K}_g$) can be selected for a single θ, and the result is automatically suitable for other wave directions. Also note, in Table I, that the *actual* energy production varies with θ, which relates to the well-known WEC array *layout optimization* problem [11]. However, in the studied case, the energy variation with θ is less than 2%, whose influencing factors include wave irregularity, viscous force, and device constraints [35].

TABLE II
NORMALIZED ENERGY PRODUCTION PERFORMANCE OF R-CMPC (UPPER) AND DMPC (LOWER)

R-CMPC	H_s=0.5 m	H_s=0.8 m	H_s=1.1 m	H_s=1.4 m
T_p=4 s	1.00 (40.0)	1.00 (38.4)	0.99 (40.5)	0.99 (41.8)
T_p=5 s	1.00 (39.2)	0.99 (40.3)	0.99 (42.0)	0.99 (43.0)
T_p=6 s	0.98 (39.9)	0.99 (40.1)	0.99 (42.1)	0.99 (43.1)
T_p=7 s	0.98 (39.5)	0.98 (39.8)	0.99 (41.1)	0.99 (42.7)

DMPC	H_s=0.5 m	H_s=0.8 m	H_s=1.1 m	H_s=1.4 m
T_p=4s	0.82 (16.0)	0.83 (15.9)	0.85 (16.3)	0.87 (16.9)
T_p=5s	0.67 (15.7)	0.75 (16.4)	0.84 (17.5)	0.91 (18.2)
T_p=6s	0.70 (15.9)	0.85 (17.0)	0.92 (17.9)	0.94 (18.5)
T_p=7s	0.82 (16.2)	0.90 (16.7)	0.94 (17.7)	0.96 (18.4)

In the brackets: the multiples of computation speed improvement for R-CMPC or DMPC compared to ideal CMPC.

E. Comprehensive Testing of Performance and Computation

Comprehensive testing results of R-CMPC and DMPC performance and computation speed, under different sea states, are summarized in Table II, where each number is the average result under four different wave directions. The energy performance of R-CMPC, with sea-state-dependent rollout coefficient tuning, is very close to the ideal in all sea states, while a significant, about *40 times* computation speedup is achieved. On the other hand, DMPC performs poorly, and its computation speed is not as fast as R-CMPC.

F. Control Sensitivity to Non-Ideal Wave Excitation Force Estimation and Forecasting

In practice, both conventional CMPC and R-CMPC are subject to w estimation and prediction errors. The design purpose of R-CMPC is to approach ideal CMPC performance in a computationally efficiently way and, since the planning process of R-CMPC is different from conventional CMPC, it is worth studying if R-CMPC may have different sensitivity to estimation and forecast errors. To this end, first, the non-ideal, global w forecaster based on a linear DMS model, as described in Section III-B, is included, while estimation is assumed ideal. In obtaining the forecaster, wave excitation force time series samples are first generated, and a least-square method is then used to identify the linear forecaster parameters. To further study the impact of forecast errors, the accuracy of the forecaster is modulated by adding white noises into the forecaster training data, so that the noise-to-signal ratio (NSR), defined as the ratio of noise variance to the signal variance (in dB), can serve as an indicator for prediction accuracy: a higher NSR means a lower accuracy and vice versa. The forecasting performance with NSR $= -20$ dB and $\theta = 30^\circ$ is shown in Fig. 10. For this wave direction, the waves first arrive at Body 3, then Body 4, Body 2, and finally Body 1. Consequently, it can be seen that the prediction accuracy (measured by goodness of fit, as defined in [27]) is in *reverse* order, with the down-wave Body 1 enjoying highest accuracy, since up-wave information from Bodies 2-4 are intrinsically incorporated in a global forecaster.

The control results are shown in Fig. 11. One can see that the controlled energy production decreases as the prediction

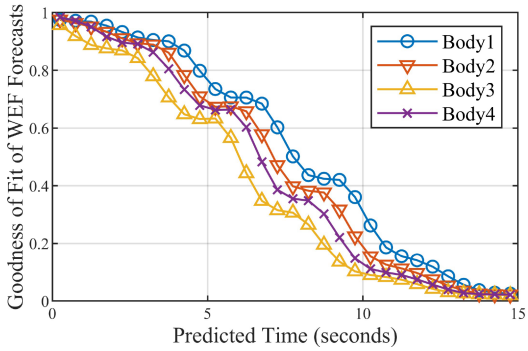

Fig. 10. Goodness of fit of a global forecaster under wave direction $\theta = 30^\circ$.

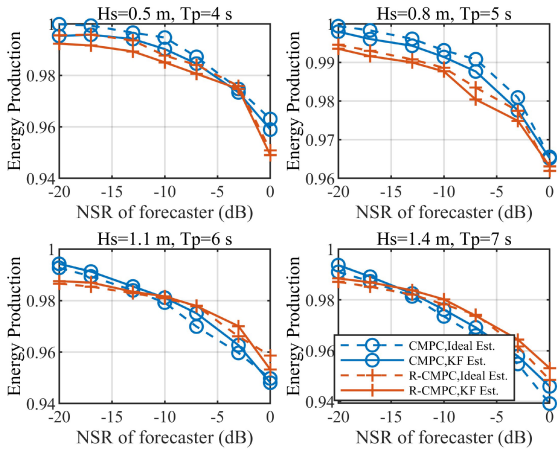

Fig. 11. Sensitivity of CMPC and R-CMPC performance (normalized against the ideal CMPC with no w error) to wave excitation force forecast errors (which increase with NSR).

error increases. Conventional CMPC and R-CMPC generally have similar sensitivity characteristics, and with a relatively accurate forecaster (NSR $= -20$ dB), performance degradation, compared with the ideal case, is very limited (less than 2%). Note that, irrespective of the NSR value, the forecasting accuracy typically decreases with the forecast horizon length, and the *insensitivity* of both conventional CMPC and R-CMPC when NSR $= -20$ dB may be explained by the fact that MPC relies more on the accuracy of w information in the near future, than in a more distant future.

Then, the non-ideal, global w estimator, based on a KF, as described in Section III-B, is further included. The random-walk KF is manually programmed directly following [26], with covariance parameters tuned according to the guidelines in [36]. The results are shown in Fig. 11. It can be seen that non-ideal estimation does lead to performance degradation in most cases, but this effect is very limited, since a global estimator, with the complete system model, can reach high accuracy [27].

In addition, the DMPC sensitivity results are shown in Fig. 12, where independent estimators and forecasters, as described in Section III-B, are further included. In general, DMPC performance is consistently lower than CMPC and R-CMPC, and under each estimation-forecast option, DMPC sensitivity to forecast errors is rather unpredictable. However, it can be seen

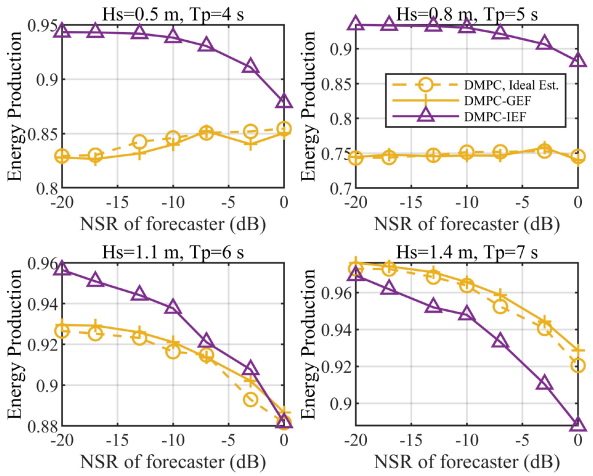

Fig. 12. Sensitivity of DMPC performance (normalized against the ideal CMPC with no w error) to wave excitation force forecast error (which increase with NSR). GEF/IEF: global/independent estimation and forecast.

that DMPC, with independent w estimation and prediction, sometimes performs better than DMPC with global estimation and prediction. Mutual radiation is not modeled in the decentralized estimator, so its estimate will be the *sum* of the incident wave excitation force and mutual radiation forces from other bodies, as revealed in [36]. At the first glance, this obviously introduces an estimation error. For DMPC, however, this turns out to be an advantage, since now the device is controlled to make use of the *total* external wave forces, rather than a part of it (the actual wave excitation force). Hence, performance degradation of DMPC can be alleviated, particularly for small waves. This interesting phenomenon can be viewed as an extension to the model error sensitivity analysis in [36].

VI. Conclusion

In this paper, a fast R-CMPC controller is proposed for WEC arrays. The novel controller adopts the idea of only optimizing the first few control moves in MPC planning, while rolling out the remaining system trajectories using a pre-determined controller. A linear, 2-DoF controller, with a sea-state-dependent coefficient tuning strategy, is further proposed to serve as the rollout controller. The proposed R-CMPC is tested in a simulation example of a 4-body WEC array, under a realistic range of sea states. While conventional CMPC requires a relatively long optimization horizon to reach optimal performance, for R-CMPC it is sufficient to only make the rollout horizon long enough, while the optimization horizon can be kept short. The energy production performance of R-CMPC is determined by the rollout control coefficients, and this relationship is dependent on the sea state, mainly on the significant wave height and peak period, and is independent of the wave direction. For each sea state, an optimal set of rollout coefficients that corresponds to the highest performance can be found, which is to be stored in a look-up table for online use. It is shown that the proposed sea-state-dependent R-CMPC controller can achieve near-optimal energy production (generally over 99% of the optimum) under all sea states while speeding up the online computation by about 40 times, compared to conventional CMPC. In addition, conventional CMPC and R-CMPC have similar sensitivity characteristics to wave excitation force estimation and forecast errors, and can both maintain close-to-ideal performance with a global KF-based estimator and a global DMS forecaster.

Some limitations of this study are worth noting. First, while R-CMPC is successful in reducing control complexity for a given array, the complexity still grows with the array size. Combining R-CMPC with *neighborhood* control approaches, which exploits the proximity relationships between devices to *limit* control complexity for arbitrarily large arrays, would be a valuable direction for future work. Meanwhile, the control is developed based on heave motion only, while actual WECs usually exhibit multi-mode motion. For devices whose motion is predominantly heave, such single-degree-of-freedom control typically remains effective [22], [37]. However, when multi-mode dynamics are more pronounced, additional control enhancements may be required, which deserves future study. Finally, this study focuses exclusively on the 'power production region' of WECs with displacement and force constraints. For more energetic sea states, under which both constraints cannot be achieved simultaneously, the device must switch to a 'protection mode'. The point at which this transition occurs is a *design* issue that needs design of a suitable supervisory controller in practical application.

References

[1] "Ocean CorPower," 2024. Accessed: Jul. 8, 2024. [Online]. Available: https://corpowerocean.com/projects/
[2] J. V. Ringwood, S. Zhan, and N. Faedo, "Empowering wave energy with control technology: Possibilities and pitfalls," *Annu. Rev. Control*, vol. 55, pp. 18–44, 2023.
[3] G. Li and M. R. Belmont, "Model predictive control of sea wave energy converters–Part II: The case of an array of devices," *Renewable Energy*, vol. 68, pp. 540–549, 2014.
[4] G. Bacelli, P. Balitsky, and J. V. Ringwood, "Coordinated control of arrays of wave energy devices—Benefits over independent control," *IEEE Trans. Sustain. Energy*, vol. 4, no. 4, pp. 1091–1099, Oct. 2013.
[5] A. C. M. O'Sullivan, W. Sheng, and G. Lightbody, "An analysis of the potential benefits of centralised predictive control for optimal electrical power generation from wave energy arrays," *IEEE Trans. Sustain. Energy*, vol. 9, no. 4, pp. 1761–1771, Oct. 2018.
[6] T. Vervaet et al., "System identification and centralised causal impedance matching control of a row of two heaving point absorber wave energy converters," *Ocean Eng.*, vol. 309, 2024, Art. no. 118399.
[7] N. Faedo et al., "Experimental assessment of combined sliding mode & moment-based control (SM ^{2} C) for arrays of wave energy conversion systems," *Control Eng. Pract.*, vol. 144, 2024, Art. no. 105818.
[8] S. Zou and O. Abdelkhalik, "Collective control in arrays of wave energy converters," *Renewable Energy*, vol. 156, pp. 361–369, 2020.
[9] M. Murai, Q. Li, and J. Funada, "Study on power generation of single point absorber wave energy converters (PA-WECs) and arrays of PA-WECs," *Renewable Energy*, vol. 164, pp. 1121–1132, 2021.
[10] S. Thomas, M. Eriksson, M. Göteman, M. Hann, J. Isberg, and J. Engström, "Experimental and numerical collaborative latching control of wave energy converter arrays," *Energies*, vol. 11, no. 11, 2018, Art. no. 3036.
[11] H. Abdulkadir and O. Abdelkhalik, "Optimization of heterogeneous arrays of wave energy converters," *Ocean Eng.*, vol. 272, 2023, Art. no. 113818.
[12] H. Abdulkadir and O. Abdelkhalik, "Optimal constrained control of arrays of wave energy converters," *J. Mar. Sci. Eng.*, vol. 12, no. 1, 2024, Art. no. 104.
[13] Z. Lin, X. Huang, X. Xiao, and J. V. Ringwood, "Fast optimal control performance evaluation for wave energy control co-design," *Renewable Energy*, vol. 239, 2025, Art. no. 121974.

[14] D. Oetinger, M. E. Magaña, and O. Sawodny, "Centralised model predictive controller design for wave energy converter arrays," *IET Renewable Power Gener.*, vol. 9, no. 2, pp. 142–153, 2015.
[15] Q. Zhong and R. W. Yeung, "Model-predictive control strategy for an array of wave-energy converters," *J. Mar. Sci. Appl.*, vol. 18, pp. 26–37, 2019.
[16] Q. Zhong and R. W. Yeung, "On optimal energy-extraction performance of arrays of wave-energy converters, with full consideration of wave and multi-body interactions," *Ocean Eng.*, vol. 250, 2022, Art. no. 110863.
[17] B. Zhang, H. Zhang, S. Yang, S. Chen, X. Bai, and A. Khan, "Predictive control for a wave-energy converter array based on an interconnected model," *J. Mar. Sci. Eng.*, vol. 10, no. 8, 2022, Art. no. 1033.
[18] Z. Zhang, J. Qin, Y. Zhang, S. Huang, Y. Liu, and G. Xue, "Cooperative model predictive control for wave energy converter arrays," *Renewable Energy*, vol. 219, 2023, Art. no. 119441.
[19] G. Bacelli and J. Ringwood, "Constrained control of arrays of wave energy devices," *Int. J. Mar. Energy*, vol. 3, pp. e53–e69, 2013.
[20] S. Zhan, Y. Chen, J. Lan, and Y. Zhang, "Energy maximisation control for an array of wave energy converters-a distributed approach," in *Proc. UKACC 14th Int. Conf. Control*, Winchester, U.K., 2024, pp. 31–36.
[21] Z. Lin, X. Huang, and X. Xiao, "A novel model predictive control formulation for wave energy converters based on the reactive rollout method," *IEEE Trans. Sustain. Energy*, vol. 13, no. 1, pp. 491–500, Jan. 2022.
[22] Z. Lin, X. Huang, and X. Xiao, "Experimental validation of rollout-based model predictive control for wave energy converters on a two-body, taut-moored point absorber prototype," *Proc. Eur. Wave Tidal Energy Conf.*, Bilbao, Spain, 2023, vol. 15, no. 174, pp. 1–7.
[23] D. R. Herber and J. T. Allison, "Approximating arbitrary impulse response functions with prony basis functions," University of Illinois Urbana-Champaign, Tech. Rep. UIUC-ESDL-2019-01, 2019.
[24] Z. Lin, J. Zhou, X. Huang, K. Chen, X. Xiao, and J. V. Ringwood, "On loss-aware optimal control of wave energy converters with electrical power take-offs," *IEEE Trans. Sustain. Energy*, vol. 15, no. 4, pp. 2209–2218, Oct. 2024.
[25] X. Huang, Z. Lin, K. Chen, J. Zhou, and X. Xiao, "Improving wave-to-wire efficiency of direct-drive wave energy converters with loss-aware model predictive control and variable DC voltage control," *IEEE Trans. Ind. Electron.*, vol. 72, no. 2, pp. 1561–1570, Feb. 2025.
[26] Y. Peña-Sanchez, C. Windt, J. Davidson, and J. V. Ringwood, "A critical comparison of excitation force estimators for wave-energy devices," *IEEE Trans. Control Syst. Technol.*, vol. 28, no. 6, pp. 2263–2275, Nov. 2020.
[27] Y. Pena-Sanchez, M. Garcia-Abril, F. Paparella, and J. V. Ringwood, "Estimation and forecasting of excitation force for arrays of wave energy devices," *IEEE Trans. Sustain. Energy*, vol. 9, no. 4, pp. 1672–1680, Oct. 2018.
[28] Y. Pena-Sanchez, A. Mérigaud, and J. V. Ringwood, "Short-term forecasting of sea surface elevation for wave energy applications: The autoregressive model revisited," *IEEE J. Ocean. Eng.*, vol. 45, no. 2, pp. 462–471, Apr. 2020.
[29] E. F. Camacho and C. Bordons, *Model Predictive Control*. London, U.K.: Springer-Verlag, 2007.
[30] D. Silver et al., "Mastering the game of Go with deep neural networks and tree search," *Nature*, vol. 529, no. 7587, pp. 484–489, 2016.
[31] S. A. Sirigu, G. Bracco, M. Bonfanti, P. Dafnakis, and G. Mattiazzo, "On-board sea state estimation method validation based on measured floater motion," *IFAC-PapersOnLine*, vol. 51, no. 29, pp. 68–73, 2018.
[32] M. Ancellin and F. Dias, "Capytaine: A python-based linear potential flow solver," *J. Open Source Softw.*, vol. 4, no. 36, 2019, Art. no. 1341.
[33] Z. Lin, X. Huang, and X. Xiao, "Approximate dynamic programming for control of wave energy converters with implementation and validation on a point absorber prototype," *IEEE Trans. Ind. Electron.*, vol. 71, no. 5, pp. 4753–4761, May 2024.
[34] A. Altman and J. Gondzio, "Regularized symmetric indefinite systems in interior point methods for linear and quadratic optimization," *Optim. Methods Softw.*, vol. 11, no. 1-4, pp. 275–302, 1999.
[35] A. Babarit, "On the park effect in arrays of oscillating wave energy converters," *Renewable Energy*, vol. 58, pp. 68–78, 2013.
[36] Z. Lin, X. Huang, X. Xiao, and J. V. Ringwood, "A sensitivity analysis of wave energy converter model predictive control systems with wave excitation force estimation and prediction," *IEEE Trans. Control Syst. Technol.*, vol. 33, no. 1, pp. 136–147, Jan. 2025.
[37] N. Faedo, F. Carapellese, E. Pasta, and G. Mattiazzo, "On the principle of impedance-matching for underactuated wave energy harvesting systems," *Appl. Ocean Res.*, vol. 118, 2022, Art. no. 102958.

Zechuan Lin was born in Fujian Province, China, in 1996. He received the B.E. degree in electrical engineering from North China Electrical Power University, Beijing, China, in 2019, and the Ph.D. degree in electrical engineering from Tsinghua University, Beijing, in 2024. He is currently a Research Assistant with the Department of Electrical Engineering, Tsinghua University. From 2023 to 2024, he was with the Centre for Ocean Energy Research, Maynooth University, Kildare, Ireland, where he was a Visiting Student. His research interests include wave energy generation and electrical machine control.

Xuanrui Huang was born in Xinjiang Province, China, in 1991. He received the B.E. and Ph.D. degrees in electrical engineering from Tsinghua University, Beijing, China, in 2013 and 2020, respectively, where he is currently a Postdoctor with the Department of Electrical Engineering. His research interests include permanent-magnet synchronous motor control, wave energy, and switched reluctance machines.

Yifei Han was born in Shandong Province, China, in 2002. She received the B.E. degree in 2024 from Tsinghua University, Beijing, China, where she is currently working toward the Ph.D. degree. Her research focuses on wave energy converter arrays.

Xi Xiao (Member, IEEE) was born in Hunan Province, China, in 1973. He received the B.E., M.E., and Ph.D. degrees in electrical engineering from Saint Petersburg State Technical University, Saint Petersburg, Russia, in 1995, 1997, and 2000, respectively. Since 2001, he has been with the Department of Electrical Engineering, Tsinghua University, Beijing, China, where he is currently a Full Professor. His main research interests include permanent magnet synchronous motor control, power electronics, and renewable energy.

John V. Ringwood (Fellow, IEEE) received the Diploma in electrical engineering from the Technological University, Dublin, Ireland, in 1981, and the Ph.D. degree in control systems from Strathclyde University, Glasgow, U.K., in 1985. From 1985 to 2000 he was with the School of Electronic Engineering, Dublin City University, Dublin, and was a Visiting positions with Massey University, Auckland, New Zealand, and The University of Auckland, Auckland. He is currently the Chair Professor of Electronic Engineering and the Director of the Centre for Ocean Energy Research, Maynooth University, Kildare, Ireland. He was the Founding Head of the Department of Electronic Engineering with Maynooth University and was a Dean of Engineering from 2001-2006. He has coauthored the monograph Hydrodynamic Control of Wave Energy Devices (with Umesh Korde). His research interests include control systems and its applications, including renewable energy systems (and wave energy in particular), physiology, and exercise physiology. Dr. Ringwood was corecipient of IEEE 2016 Control Systems Outstanding Paper Award, and 2023 IEEE Trans. on Control Systems Technology Outstanding Paper Award. He is currently an Associate Editor for IEEE TRANSACTION ON SUSTAINABLE ENERGY, *the Journal of Ocean Engineering and Marine Energy*, and *IET Renewable Power Generation*. He is a Chartered Engineer and a Fellow of Engineers Ireland.